Electronic Supplementary Material (ESI) for Journal of Materials Chemistry A.

Electronic Supplementary Information

Amorphous Porous Fe-BTC Prepared by the Post-Synthetic Metal-Ion Metathesis of HKUST-1

Asong Byun,[a] Dohyun Moon,[b] Byeongchan Lee,[a] and Jinhee Park*[a]

[a.] Department of Physics and Chemistry, Daegu Gyeongbuk Institute of Science and Technology (DGIST), Daegu 42988, Republic of Korea
[b.] Beamline Department, Pohang Accelerator Laboratory, Pohang 37673, Republic of Korea

Table of Contents

Part S1. General Information

1. Materials

$Cu(NO_3)_2 \cdot 3H_2O$ (98%), benzaldehyde (99%), trimethylsilyl cyanide (98%), nitric acid (70%), and anhydrous dichloromethane (99.8%) were procured from Sigma Aldrich. $Zn(NO_3)_2 \cdot 6H_2O$ (99%), $FeCl_2 \cdot 4H_2O$ (99%), $Fe(NO_3)_3 \cdot 9H_2O$ (98+%), benzaldehyde dimethyl acetal (99%), malononitrile (99%), tetrafluoroboric acid (ca. 50% w/w aq. soln.), *N,N*-dimethylformamide (DMF) (99.8%), and anhydrous acetonitrile (99.8+%) were obtained from Alfa Aesar. Dimethyl sulfoxide-d_6 (99.9%) and chloroform-*d* (d, 99.8%) (99.5%) were purchased from Cambridge Isotope Laboratories. Acetonitrile-d_3 (d, 99%) was bought form Acros Organics. Potassium bromide was purchased from Uvasol. Anhydrous ethanol (EtOH) (99%), dichloromethane (DCM) (99%), and acetonitrile (ACN) (99.5%) were purchased from Daejung Chemical. All commercial chemicals were used without further purification.

2. Measurements

Proton nuclear magnetic resonance (^{1}H-NMR) spectra were measured on a Fourier transform nuclear magnetic resonance spectrometer from Bruker (AVANCE III 400). Chemical shifts are reported in ppm downfield referenced against NMR solvents, DMSO-d_6 (δ = 2.50), chloroform-*d* (δ = 7.26), and acetonitrile-d_3 (δ = 1.94). Powder X-ray diffraction (PXRD) data were obtained from a Empyrean X-ray diffractometer (Panalytical) with Cu *K*α radiation ($\lambda_{K\alpha1}$ = 1.541 Å, 40 kV, and 30 mA). Inductively coupled plasma-optical emission spectrometry (ICP-OES) data were obtained by ICAP7400DUO (Thermo Scientific). Scanning electron microscopy (SEM) images were collected using SU8230, SU8020, and S-4800 from Hitachi. Ltd., operating at 1.5, 3, and 15 kV with 10 μA. Gas sorption isotherms were obtained using Brunauer-Emmett-Teller (BET) analyzers from Soletek (BELSORP-max) and Micromeritics Instrument Corporation (3-Flex). Fourier transform infrared (FT-IR) spectra were collected by a Nicolet Continuum FT-IR spectrometer (Thermo Scientific). Thermogravimetric analysis (TGA) data were obtained by Auto Q500 from TA instruments. Elemental analysis (EA) was performed using Vario MICRO Cube (Elementar). X-ray photoelectron spectroscopy (XPS) analyses were conducted using a Thermo Scientific ESCALAB 250Xi instrument with a monochromatized Al *K*α line source. High-resolution transmission electron microscopy (HR-TEM) images and selected area electron diffraction (SAED) pattern were collected using a Themis Z from Thermo Scientific, operating at 300 kV with a 230 mm camera length.

Part S2. Experimental Procedures

1. Synthesis of Cu-HKUST-1

Cu-HKUST-1 was synthesized according to the previously reported procedure.[1] $Cu(NO_3)_2{\cdot}3H_2O$ (4348.8 mg, 18 mmol) and H_3BTC (2521.7 mg, 12 mmol) were dissolved in 180 mL of a mixed solvent (DMF/EtOH/H_2O, 1:1:1, (v/v/v)). Tetrafluoroboric acid (ca 50% w/w aq. soln.) (3.6 g, 0.041 mol) was added to the mixture solution. Then, the solution was sonicated for 30 min to obtain the clear solution. The resulting solutions was heated at 85 °C for 2 d. The bluish and octahedral crystals were collected, washed with DMF, EtOH, and DCM and dried under reduced pressure at 120 °C for 1 d.

2. Synthesis of Zn-HKUST-1

Zn-HKUST-1 was synthesized according to the previously reported procedure with slight modifications.[2] $Zn(NO_3)_2{\cdot}6H_2O$ (148.7 mg, 0.5 mmol), and H_3BTC (105.1 mg, 0.5 mmol) were dissolved in DMF (20 mL). The solution was sonicated for 10 min to obtain the clear solution and then, heated at 70 °C for 4 d. The resulting colorless and cubic crystals were washed with DMF, EtOH, and DCM and dried under reduced pressure at 60 °C for 1 d.

3. Synthesis of $Cu_{0.50}Zn_{0.50}$-HKUST-1

$Cu(NO_3)_2{\cdot}3H_2O$ (19.81 mg, 0.082 mmol) and $Zn(NO_3)_2{\cdot}6H_2O$ (243.35 mg, 0.818 mmol) were dissolved in DMF (15 mL). H_3BTC (189.13 mg, 0.9 mmol) was dissolved in DMF (10 mL). After sonication for 10 min, tetrafluoroboric acid (ca 50% w/w aq. soln.) (197.8 µL) was added to the metal-ion solution. The two solutions were mixed together and then heated at 80 °C for 1 d. The resulting bluish and octahedral crystals were collected, washed with DMF, EtOH, and DCM and then, dried under reduced pressure at 60 °C for 1 d. Elemental analysis. Calc. (%) for $Cu_{0.50}Zn_{0.50}$-HKUST-1: C, 46.15; H, 15.38; O, 30.77; Cu, 3.85; Zn, 3.85. Found: C, 37.20; H, 24.35; Cu, 3.28; Zn, 3.27 (Cu and Zn from ICP-OES analysis).

4. Preparation of Fe-BTC

$FeCl_2{\cdot}4H_2O$ (0.2 M) and $Fe(NO_3)_3{\cdot}9H_2O$ (0.2 M) DMF solutions were prepared in an Ar-filled glove box, sonicated to obtain the clear solutions and then, filtered using a syringe filter (PTFE 0.45 µm/25 mm) to remove insoluble particles. As-synthesized $Cu_{0.50}Zn_{0.50}$-HKUST-1 crystals were washed with DMF over six times. The crystals soaked in DMF were bubbled with N_2 gas for 1 h, and then placed in the glove box.

DMF of $Cu_{0.50}Zn_{0.50}$-HKUST-1 was decanted and the mixed solution of 0.2 M $FeCl_2{\cdot}4H_2O$ (19 mL) and 0.2 M $Fe(NO_3)_3{\cdot}9H_2O$ (1 mL) was added to the crystals. The mixture was heated at 80 °C for 2 d. Orangish octahedral particles (Fe-BTC) were collected, washed with DMF, EtOH, and DCM and then, dried under reduced pressure at 80 °C for 1 d. Elemental analysis. Found (%) for Fe-BTC: C, 33.78; H, 30.35; Fe, 5.04; Cu, 0.00; Zn, 0.00 (Fe, Cu and Zn from ICP-OES analysis).Cu-HKUST-1 was synthesized according to the previously reported procedure.[1]

5. Catalytic reactions

All MOF catalysts were activated using the procedure described above, with an equal molar quantity of 0.017 mmol. Specifically, Fe-BTC (10 mg), Cu-HKUST-1 (10.25 mg), and $Cu_{0.50}Zn_{0.50}$-HKUST-1 (10.4 mg) were prepared and used as catalysts in the respective reactions: cyanosilylation, deacetalization, and Knoevenagel condensation, which are described below.

For the cyanosilylation reaction, a mixture of benzaldehyde (1 mmol), trimethylsilyl cyanide (1.2 mmol), anhydrous DCM (3 mL), and the catalyst was prepared in an open-top 4 mL vial in an Ar-filled glovebox. The reaction mixture was homogeneously mixed using an incubated shaker at 25 °C. Kinetic profiles as a function of reaction duration were obtained by mixing two drops of the reaction solution with 0.45 mL of chloroform-*d*, followed by NMR analysis.

For the deacetalization reaction, a mixture of benzaldehyde dimethyl acetal (1 mmol), distilled water (1 mmol), anhydrous ACN (2 mL), and the catalyst was prepared in a 4 mL vial under ambient conditions. The reaction mixture was homogeneously mixed using an incubated shaker at 50 °C. Kinetic profiles as a function of reaction duration were obtained by mixing two drops of the reaction solution with 0.45 mL of acetonitrile-d_3, followed by NMR analysis.

For the Knoevenagel condensation reaction, a mixture of benzaldehyde (1 mmol), malononitrile (1.05 mmol), anhydrous ACN (2 mL), and the catalyst was prepared, and the subsequent procedures were carried out following the same method described above.

The reusability of the catalysts was tested by subjecting them to an abundant washing process with each fresh reaction solvents (DCM or ACN) after each cycle. The contaminated solvents were carefully decanted, and the catalysts were subsequently reused in the recycling tests.

Part S3. Optimization of Cu_xZn_{1-x}-HKUST-1

1. Optical microscopy images

Table S1 Relationship between Zn^{2+}:Cu^{2+} precursor ratio and the resulting Cu_xZn_{1-x}-HKUST-1.

Precursor ratio (Zn^{2+}:Cu^{2+})	1:1	2:1	4:1	6:1	8:1	10:1
Cu_xZn_{1-x}-HKUST-1 (Cu_xZn_{1-x})	$Cu_{0.89}Zn_{0.11}$	$Cu_{0.78}Zn_{0.22}$	$Cu_{0.63}Zn_{0.37}$	$Cu_{0.56}Zn_{0.44}$	$Cu_{0.52}Zn_{0.48}$	$Cu_{0.50}Zn_{0.50}$
Precursor ratio (Zn^{2+}:Cu^{2+})	12:1	14:1	16:1	18:1	20:1	
Cu_xZn_{1-x}-HKUST-1 (Cu_xZn_{1-x})	$Cu_{0.43}Zn_{0.57}$	$Cu_{0.39}Zn_{0.61}$	$Cu_{0.38}Zn_{0.62}$	$Cu_{0.36}Zn_{0.64}$	$Cu_{0.35}Zn_{0.65}$	

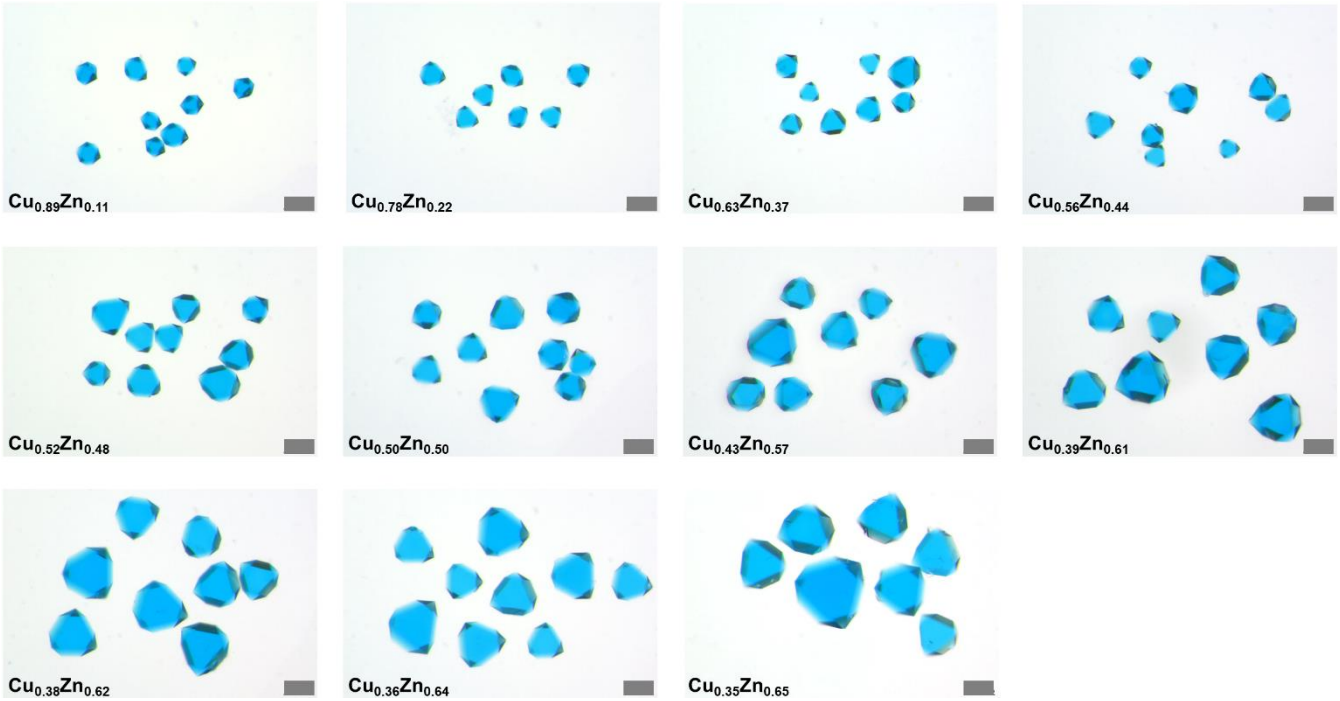

Fig. S1 Optical microscopy images of Cu_xZn_{1-x}-HKUST-1 (denoted as Cu_xZn_{1-x}). Scale bars, 100 μm.

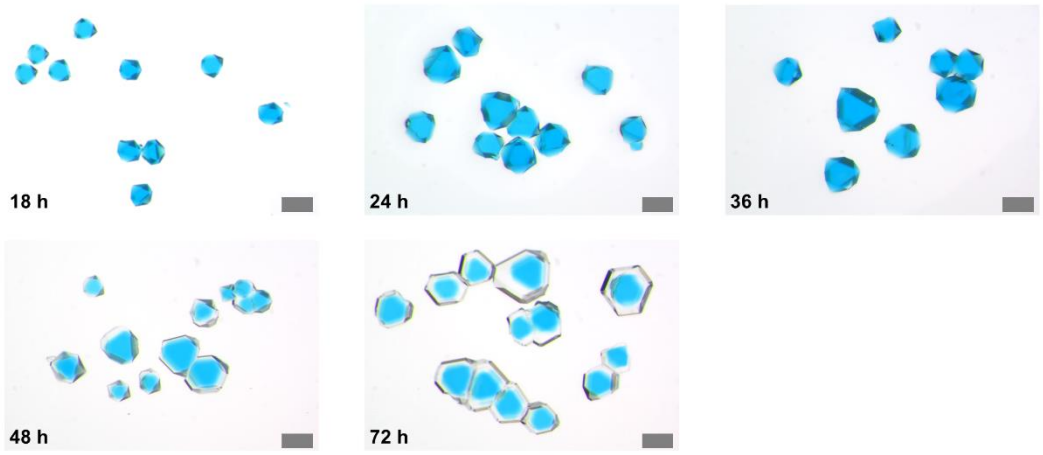

Fig. S2 Optical microscopy images of $Cu_{0.50}Zn_{0.50}$-HKUST-1 as a function of reaction time. Scale bars, 100 µm.

2. Scanning electron microscopy-energy dispersive X-ray spectrometry (SEM-EDS)

Table S2 SEM images and EDS maps of Cu_xZn_{1-x}-HKUST-1 (denoted as Cu_xZn_{1-x}). Scale bars, 20 μm.

	SEM image	EDS mapping (Cu)	EDS mapping (Zn)
$Cu_{0.89}Zn_{0.11}$	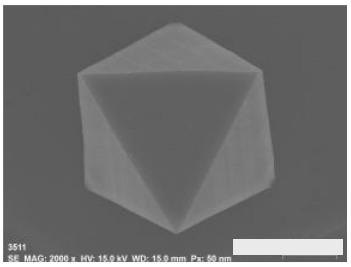	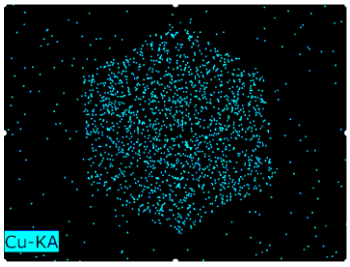	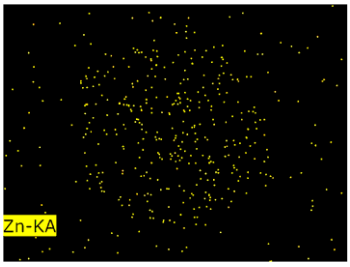
$Cu_{0.78}Zn_{0.22}$	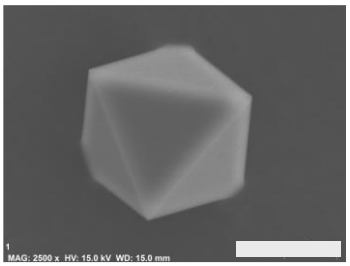	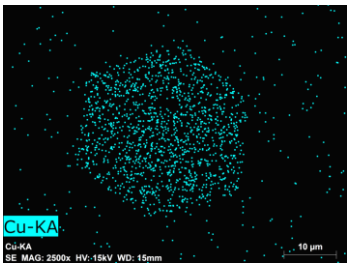	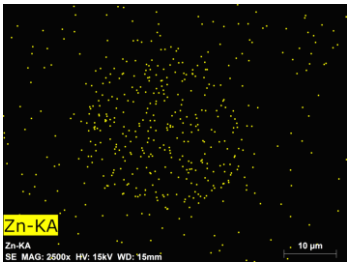
$Cu_{0.63}Zn_{0.37}$	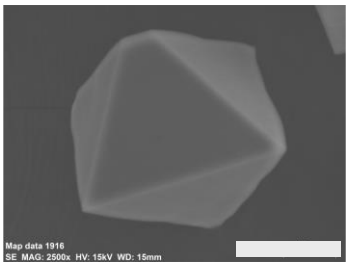	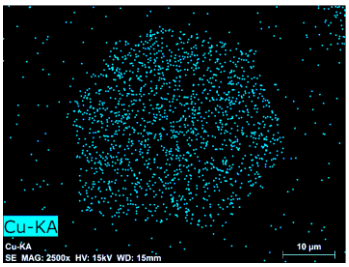	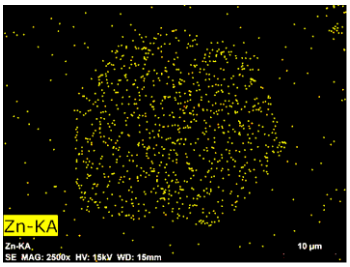
$Cu_{0.56}Zn_{0.44}$	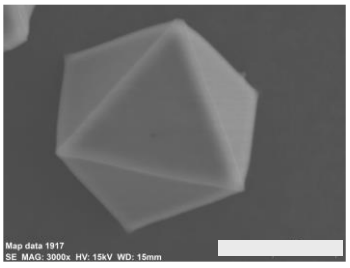	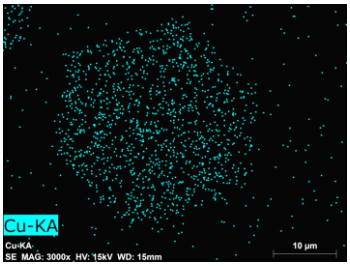	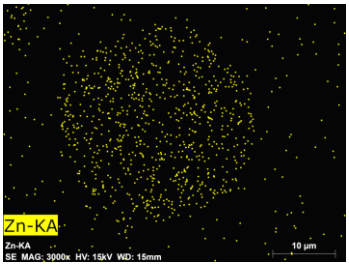
$Cu_{0.52}Zn_{0.48}$	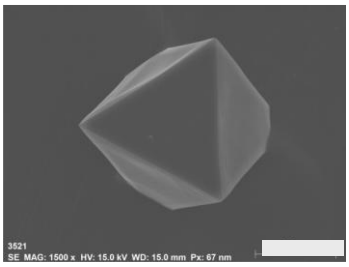	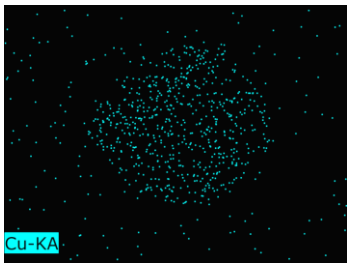	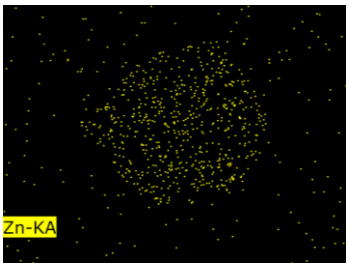

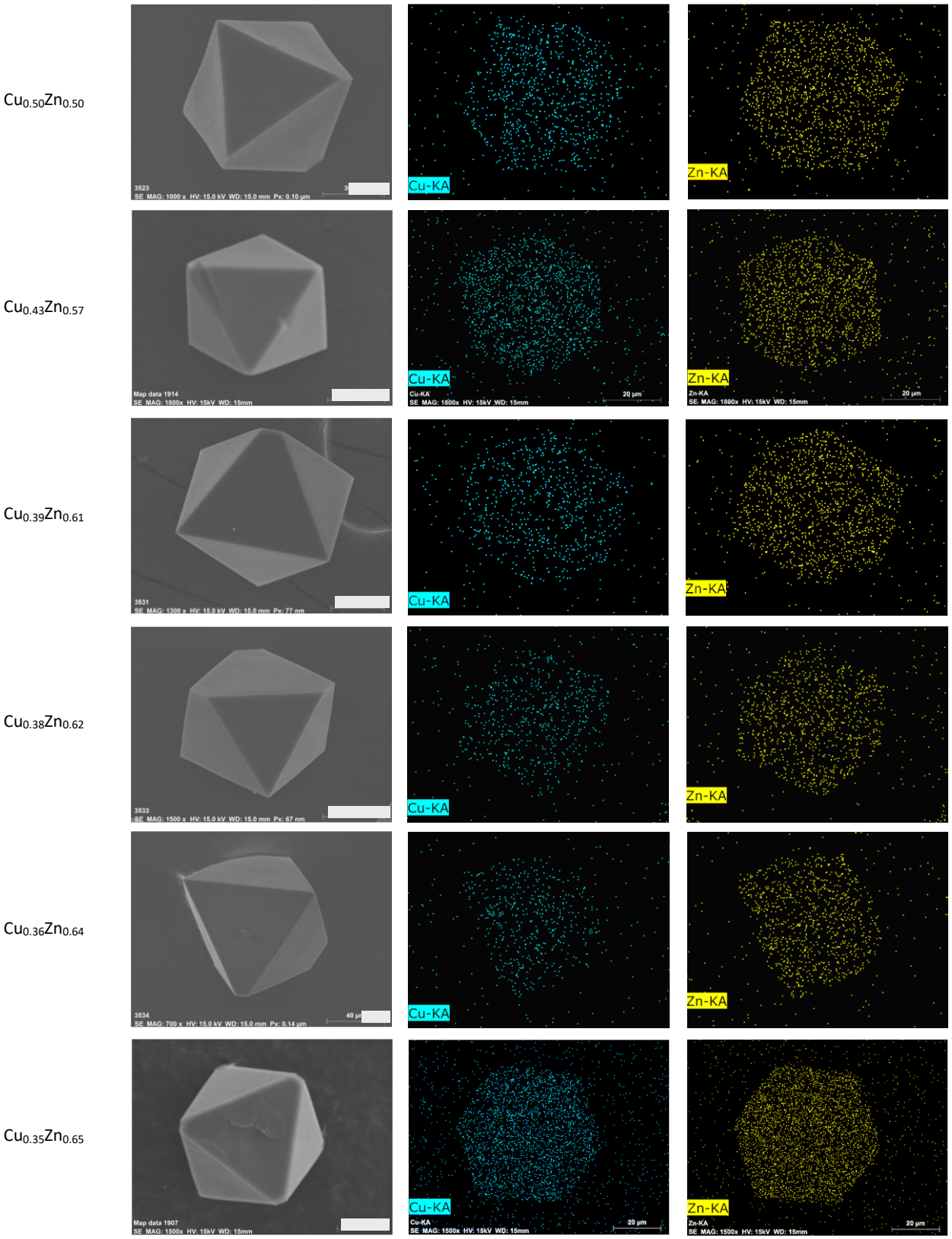
Cu0.50Zn0.50
Cu-KA
Zn-KA
Cu0.43Zn0.57
Cu-KA
Zn-KA
Cu0.39Zn0.61
Cu-KA
Zn-KA
Cu0.38Zn0.62
Cu-KA
Zn-KA
Cu0.36Zn0.64
Cu-KA
Zn-KA
Cu0.35Zn0.65
Cu-KA
Zn-KA

3. Powder X-ray diffractometry (PXRD)

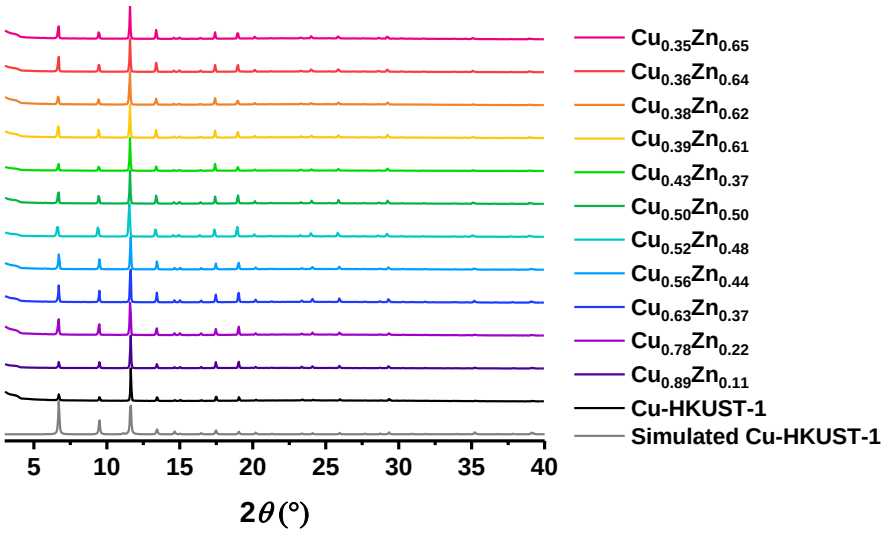

Fig. S3 PXRD patterns of as-synthesized Cu-HKUST-1 and Cu_xZn_{1-x}-HKUST-1 (denoted as Cu_xZn_{1-x}) in comparison with a simulated Cu-HKUST-1 pattern.

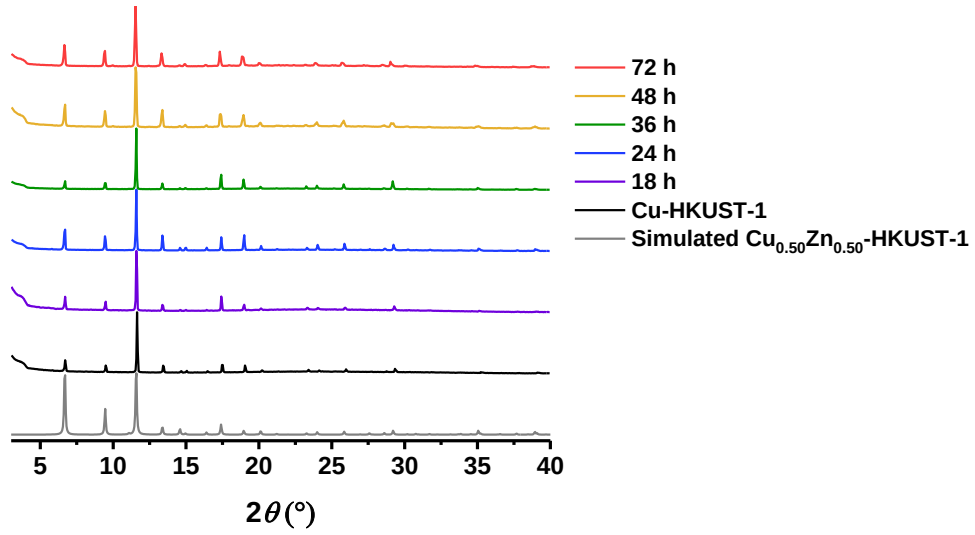

Fig. S4 PXRD patterns of as-synthesized Cu-HKUST-1 and $Cu_{0.50}Zn_{0.50}$-HKUST-1 as a function of reaction time (from 18 h to 72 h) in comparison with the simulated $Cu_{0.50}Zn_{0.50}$-HKUST-1 pattern.

4. Inductively coupled plasma-optical emission spectroscopy (ICP-OES)

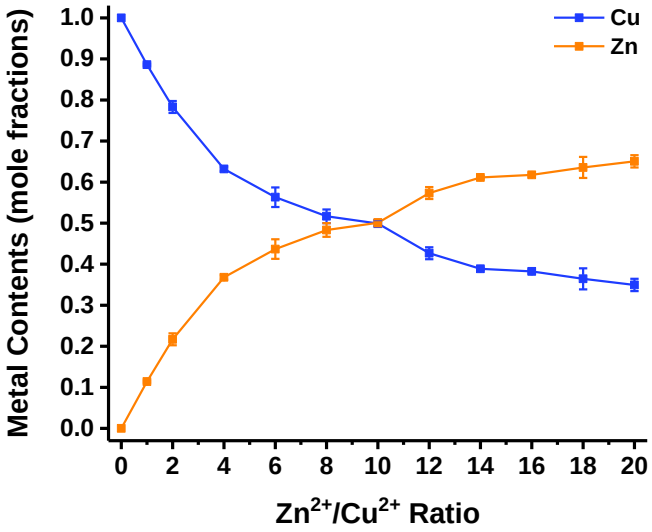

Fig. S5 Metal contents of Cu_xZn_{1-x}-HKUST-1 as a function of Zn^{2+}/Cu^{2+} precursor ratio.

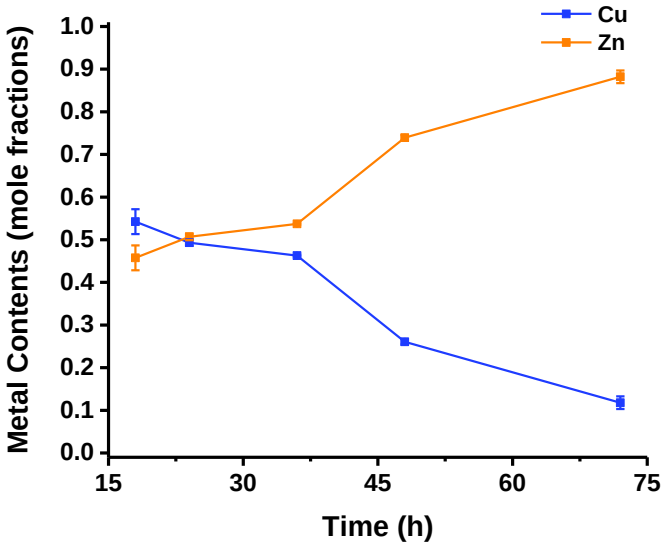

Fig. S6 Metal contents of $Cu_{0.50}Zn_{0.50}$-HKUST-1 as a function of reaction time.

Part S4. Characterizations

1. Single-crystal X-ray diffractometry (SCXRD)

The $Cu_{0.50}Zn_{0.50}$-HKUST-1 crystals were briefly washed with fresh DMF. Then, the crystals were coated with Parabar 10312 (Hampton Research Inc.) to be mounted on a micro-loop. The diffraction data of $Cu_{0.50}Zn_{0.50}$-HKUST-1 was collected by the synchrotron-based X-ray source produced from PLSII 2D bending magnet (λ = 0.7 Å) with a Si(111) double crystal monochromator and Rayonix MX225HS CCD area detector at 100 K. The diffraction frames were recorded by the PAL BL2D-SMDC program as follow conditions: detector distance of 66 mm, 1-axis omega scan; Δω of 1º, exposure time of 0.1 s/frame.[3] HKL 3000sm (ver. 720) was employed for cell refinement, reduction, and absorption correction.[4] The structure was interpreted using a SHELXT solution program with the intrinsic phasing method and refined by full-matrix least-squares on F^2 with anisotropic displacement using the SHELXL and Olex2 software package.[5] Final refinement was performed with the structural factors modified based on the disordered structural solvent electron densities obtained from the SQUEEZE routine of PLATON.

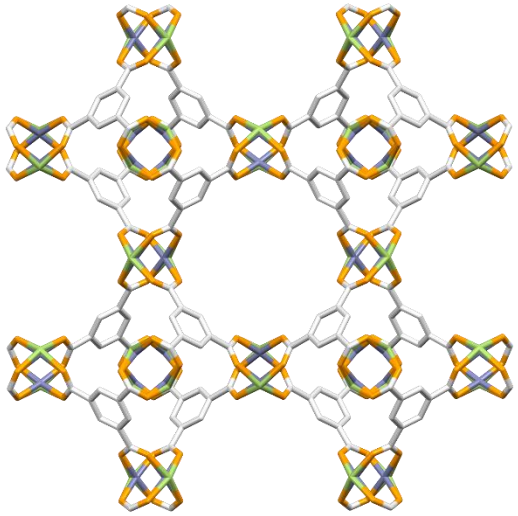

Fig. S7 Crystal structure of $Cu_{0.50}Zn_{0.50}$-HKUST-1. All hydrogen atoms and solvent molecules are omitted for clarity. Dark purple, Cu; Green, Zn; Yellow, O; Grey, C.

Table S3 Crystal structure refinement data for $Cu_{0.50}Zn_{0.50}$-HKUST-1.

Crystal nomenclature	**$Cu_{0.50}Zn_{0.50}$-HKUST-1**
Identification code	CuZn-HKUST-1_sq
CCDC number	2243907
Empirical formula	$C_6H_3O_5Cu_{0.50}Zn_{0.50}$
Formula weight	219.54
Temperature	100(2) K
Wavelength	0.700 Å
Crystal system	*Cubic*
Space group	*Fm*-3*m*
a	26.454(3) Å
b	26.454(3) Å
c	26.454(3) Å
α	90°
β	90°
γ	90°
V	18512(6) $Å^3$
Z	48
Density (calculated)	0.945 mg/m^3
Absorption coefficient	1.431 mm^{-1}
F(000)	5208
Theta range for data collection	2.515 to 26.983°
Reflections collected	37621
Independent reflections	1100 [R_{int} = 0.0898]
Completeness	98.1 %
Max. and min. transmission	1.000 and 0.976
Data / restraints / parameters	1100 / 3 / 43
Goodness-of-fit on F^2	1.075
Final *R* indices [I>2sigma(I)]	R_1 = 0.0606 wR_2 = 0.1959
***R* indices (all data)**	R_1 = 0.0634 wR_2 = 0.1991
Largest diff. peak and hole	0.420 and -0.486 e.$Å^{-3}$

2. Fe^{2+}-metathesis of $Cu_{0.50}Zn_{0.50}$-HKUST-1

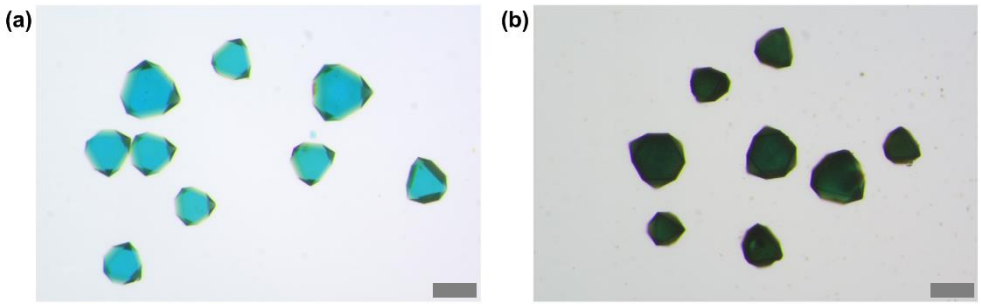

Fig. S8 Optical microscopy images of $Cu_{0.50}Zn_{0.50}$-HKUST-1 immersed in Fe^{2+} solution at 80 °C for (a) 2 d and (b) 7 d. Scale bars, 100 µm.

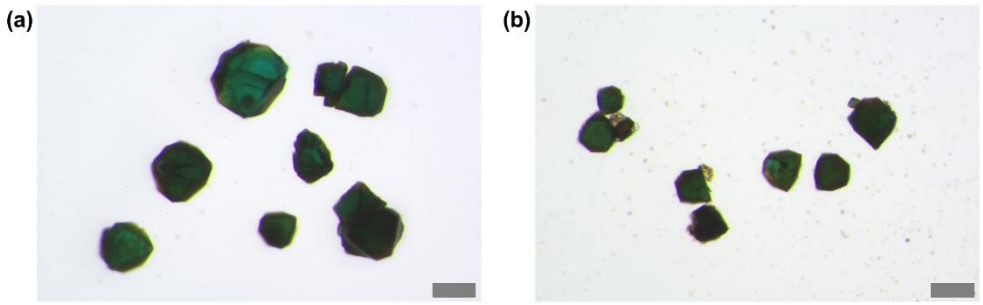

Fig. S9 Optical microscopy images of $Cu_{0.50}Zn_{0.50}$-HKUST-1 immersed in Fe^{2+} solution at 100 °C for (a) 2 d and (b) 7 d. Scale bars, 100 µm.

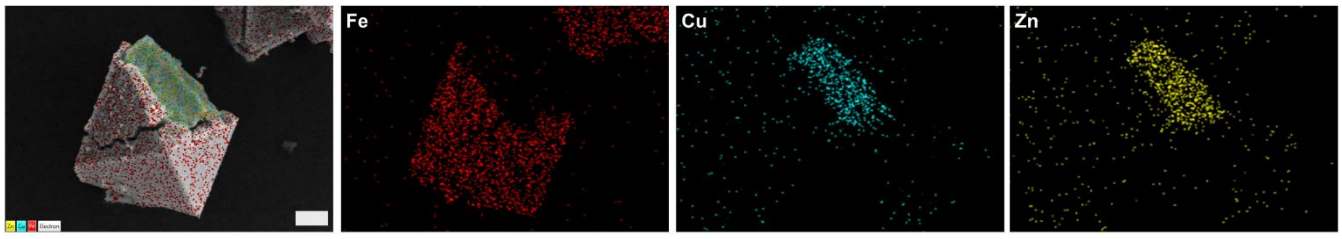

Fig. S10 EDS maps (Fe, Cu, and Zn) of $Cu_{0.50}Zn_{0.50}$-HKUST-1 after Fe^{2+} metathesis at 100 °C for 7 d. Scale bar, 10 µm.

3. Fe^{2+}/Fe^{3+}-metathesis with Cu_xZn_{1-x}-HKUST-1

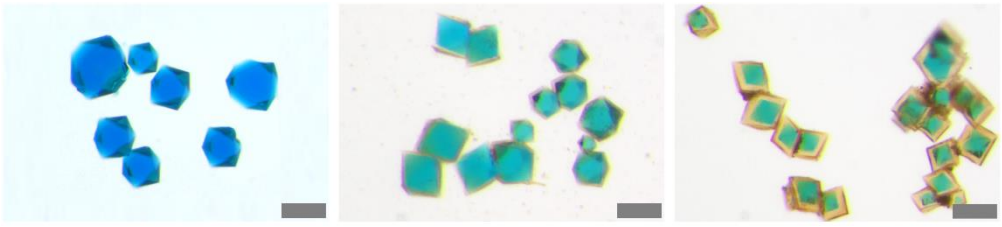

Fig. S11 Optical microscopy images of Cu-HKUST-1 (left) and Cu-HKUST-1 immersed in Fe^{2+}/Fe^{3+} solution at 80 °C for 1 d (middle) and 2 d (right). Scale bars, 100 µm.

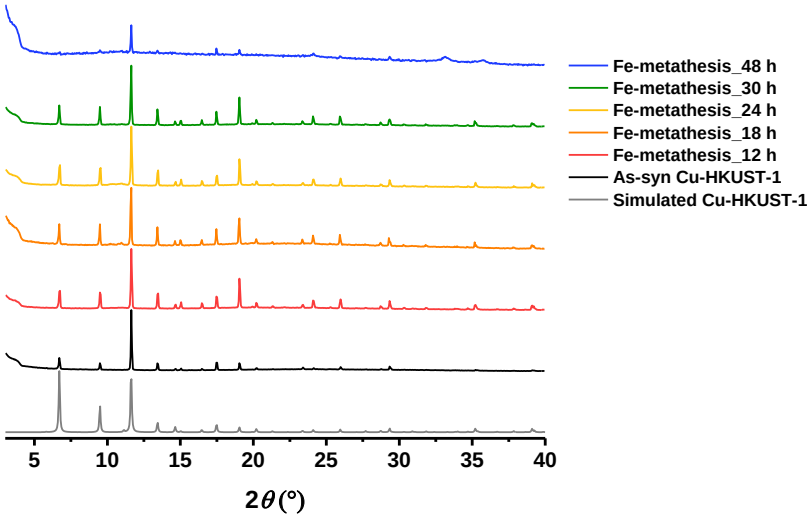

Fig. S12 PXRD patterns of Cu-HKUST-1 during Fe-metathesis in comparison with the simulated and as-synthesized Cu-HKUST-1 patterns.

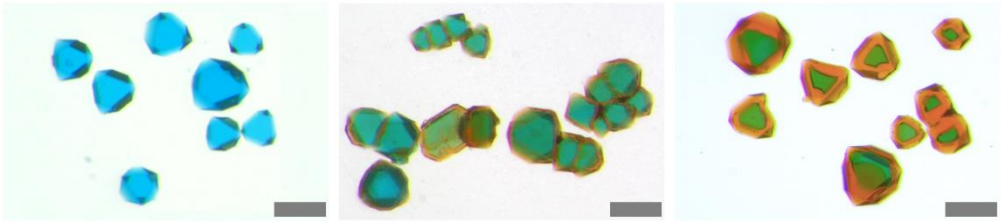

Fig. S13 Optical microscopy images of $Cu_{0.63}Zn_{0.37}$-HKUST-1 (left) and $Cu_{0.63}Zn_{0.37}$-HKUST-1 immersed in Fe^{2+}/Fe^{3+} solution at 80 °C for 1 d (middle) and 2 d (right). Scale bars, 100 µm.

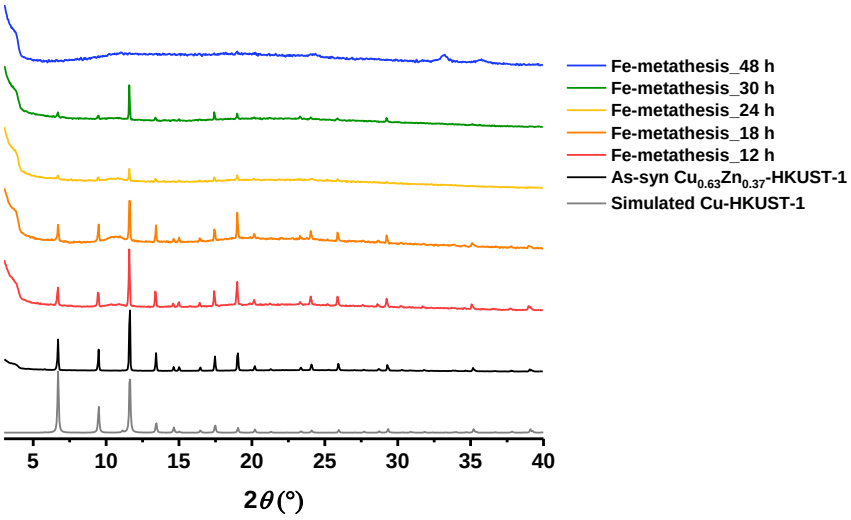

Fig. S14 PXRD patterns of $Cu_{0.63}Zn_{0.37}$-HKUST-1 during Fe-metathesis in comparison with the simulated Cu-HKUST-1 and as-synthesized $Cu_{0.63}Zn_{0.37}$-HKUST-1 patterns.

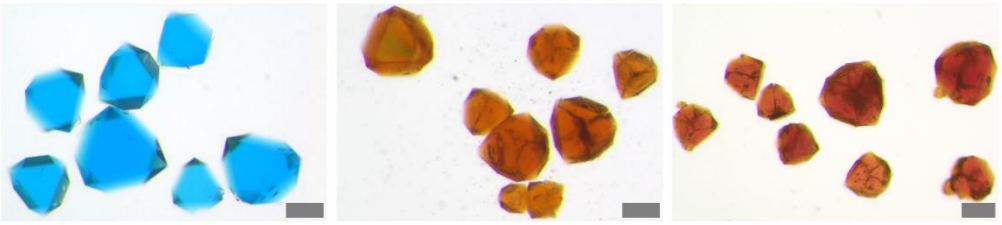

Fig. S15 Optical microscopy images of $Cu_{0.35}Zn_{0.65}$-HKUST-1 (left) and $Cu_{0.35}Zn_{0.65}$-HKUST-1 immersed in Fe^{2+}/Fe^{3+} solution at 80 °C for 1 d (middle) and 2 d (right). Scale bars, 100 µm.

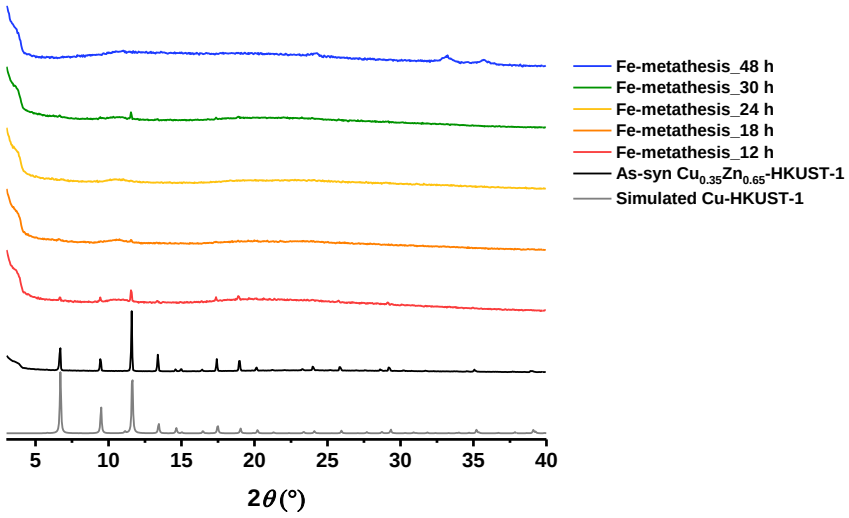

Fig. S16 PXRD patterns of $Cu_{0.35}Zn_{0.65}$-HKUST-1 during Fe-metathesis in comparison with the simulated Cu-HKUST-1 and as-synthesized $Cu_{0.35}Zn_{0.65}$-HKUST-1 patterns.

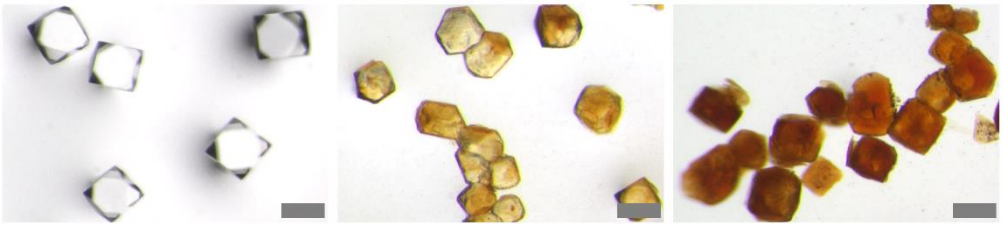

Fig. S17 Optical microscopy images of Zn-HKUST-1 (left) and Zn-HKUST-1 immersed in Fe^{2+}/Fe^{3+} solution at 80 °C for 1 d (middle) and 2 d (right). Scale bars, 100 µm.

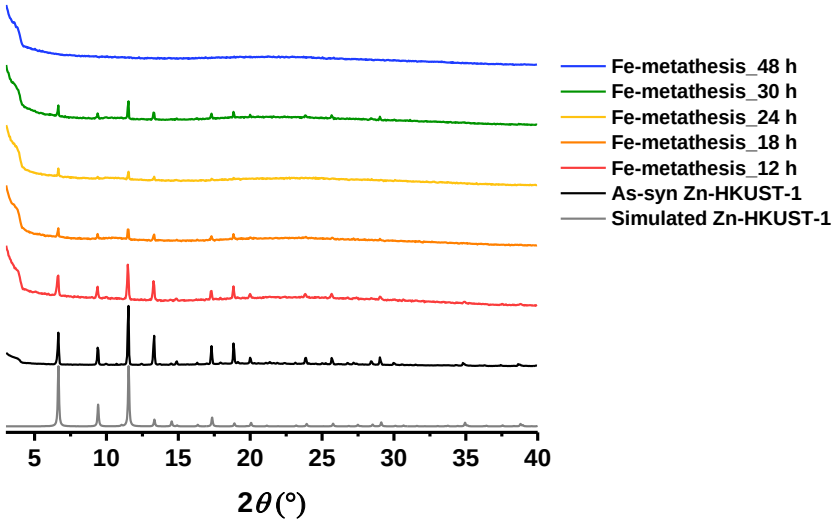

Fig. S18 PXRD patterns of Zn-HKUST-1 during Fe-metathesis in comparison with the simulated and as-synthesized Zn-HKUST-1 patterns.

4. Gas adsorption–desorption isotherms

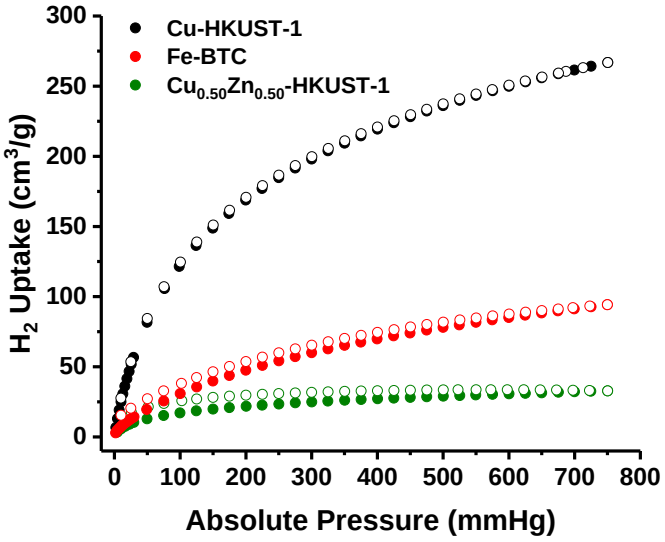

Fig. S19 H_2 adsorption–desorption isotherms (77 K) of Fe-BTC (red), Cu-HKUST-1 (black), and $Cu_{0.50}Zn_{0.50}$-HKUST-1 (green).

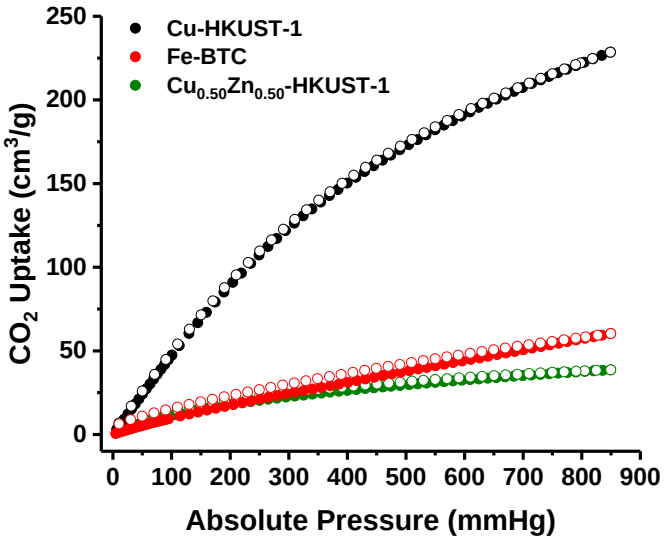

Fig. S20 CO_2 adsorption–desorption isotherms (273 K) of Fe-BTC (red), Cu-HKUST-1 (black), and $Cu_{0.50}Zn_{0.50}$-HKUST-1 (green).

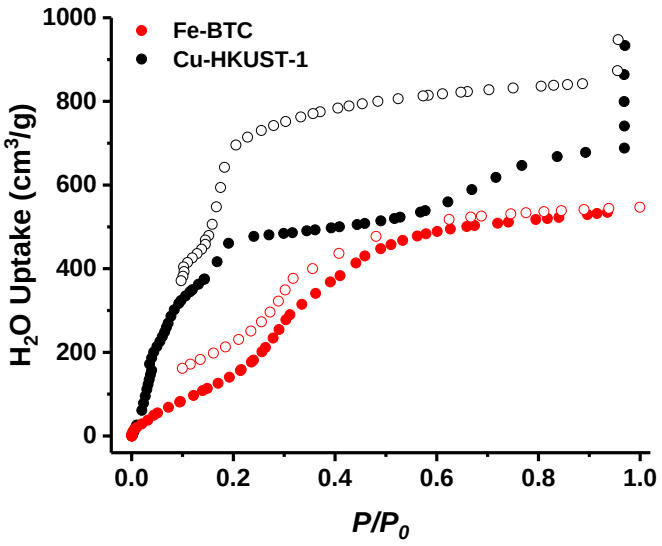

Fig. S21 H_2O adsorption–desorption isotherms (298 K) of Fe-BTC (red) and Cu-HKUST-1 (black).

5. Fe^{3+}-metathesis of $Cu_{0.50}Zn_{0.50}$-HKUST-1

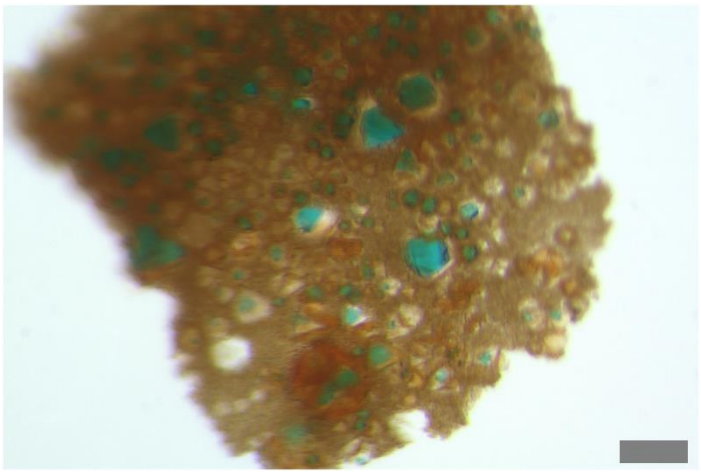

Fig. S22 Optical microscopy image of $Cu_{0.50}Zn_{0.50}$-HKUST-1 after Fe^{3+}-metathesis. Scale bar, 100 μm.

6. Thermogravimetric analysis (TGA)

At least 7 mg of a dried sample was loaded onto an aluminum pan, heated at 100 °C for 60 min and then, cooled to 25 °C. The sample was re-heated to 600 °C at a rate of 2 °C/min under a continuous N_2 flow.

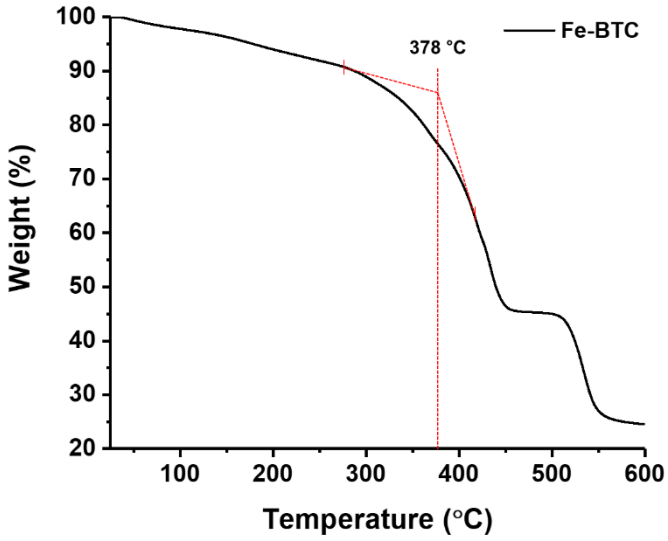

Fig. S23 TGA curve of Fe-BTC.

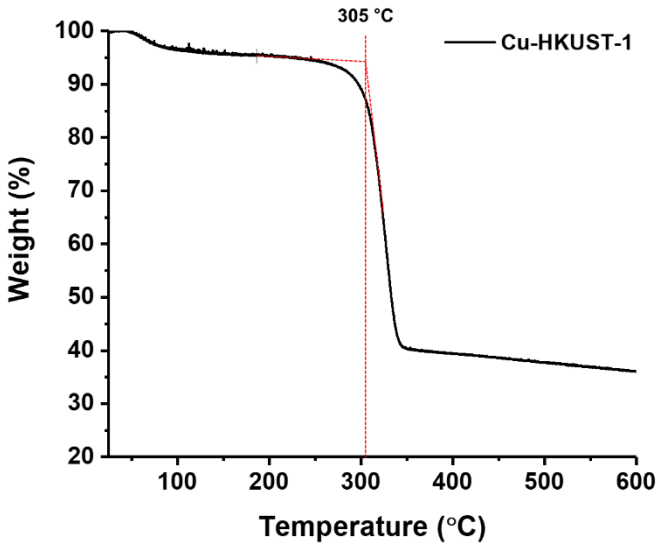

Fig. S24 TGA curve of Cu-HKUST-1.

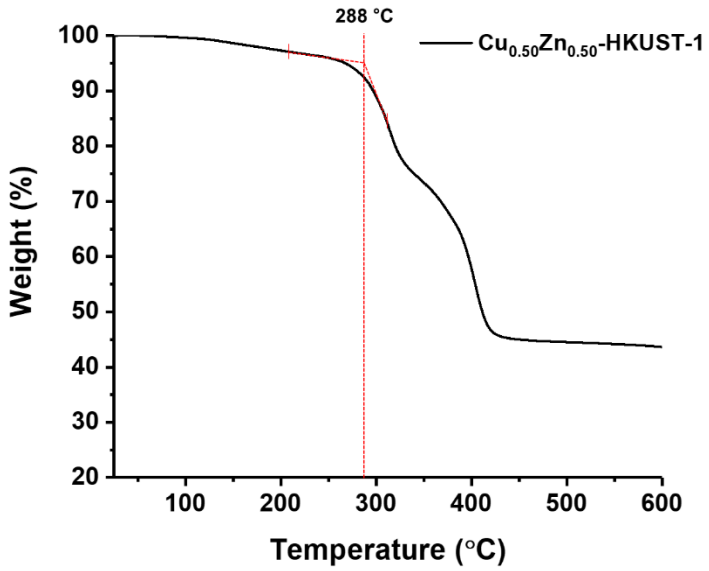

Fig. S25 TGA curve of $Cu_{0.50}Zn_{0.50}$-HKUST-1.

7. Fourier-transform infrared (FT-IR) spectroscopy

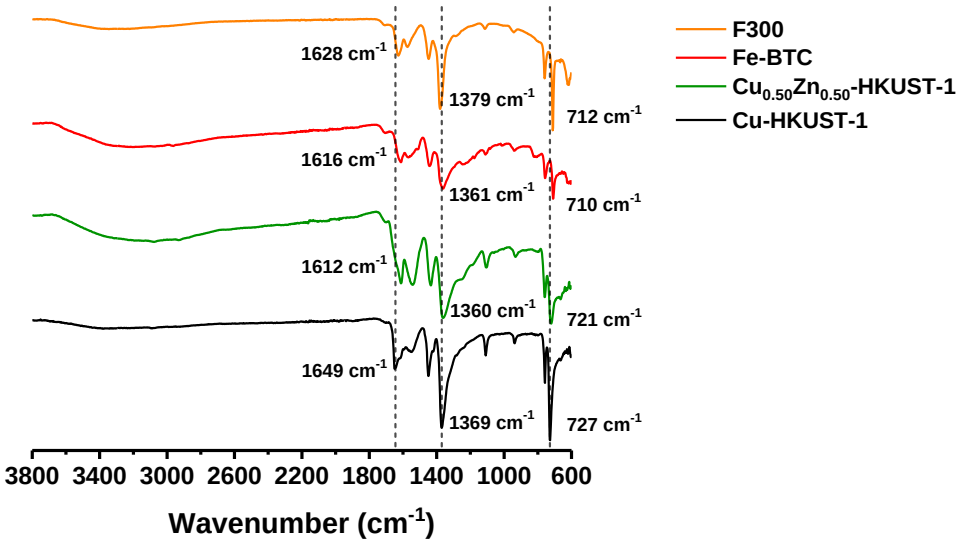

Fig. S26 IR spectra of Cu-HKUST-1 (black), $Cu_{0.50}Zn_{0.50}$-HKUST-1 (green), Fe-BTC (red), and F300 (orange). The Fe-O stretching vibrations displayed slight differences between Fe-BTC, measured at 710 cm^{-1}, and F300, estimated at 712 cm^{-1}. This implies a marginally weaker (hence longer) Fe-O coordination bond in Fe-BTC.

8. Electron paramagnetic resonance (EPR) spectroscopy

The existence of Fe^{3+} in Fe-BTC was further confirmed by an EPR spectrum in which a broad peak was observed at g = 2.02.[6, 7] EPR measurement was conducted under inert conditions. Activated Fe-BTC (5 mg) was transferred to a quartz EPR tube and the EPR spectrum was recorded at a power of 1 mW, modulation width of 1 mT, time constant of 0.03 s, conversion time of 30 s, and signal amplitude of 50-fold at room temperature.

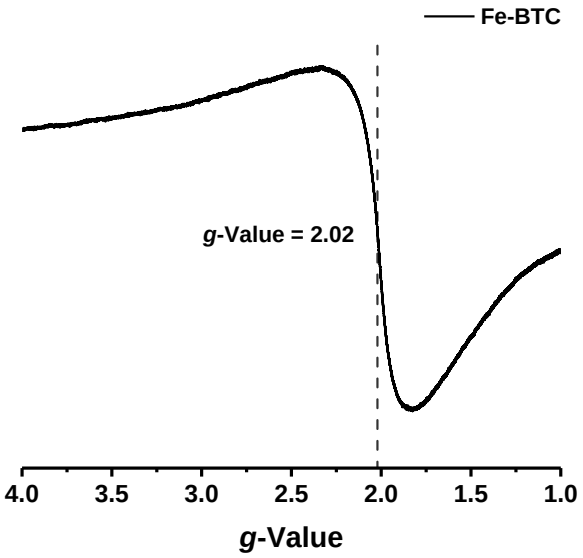

Fig. S27 EPR spectrum of Fe-BTC.

9. High-resolution transmission electron microscopy (HR-TEM) images

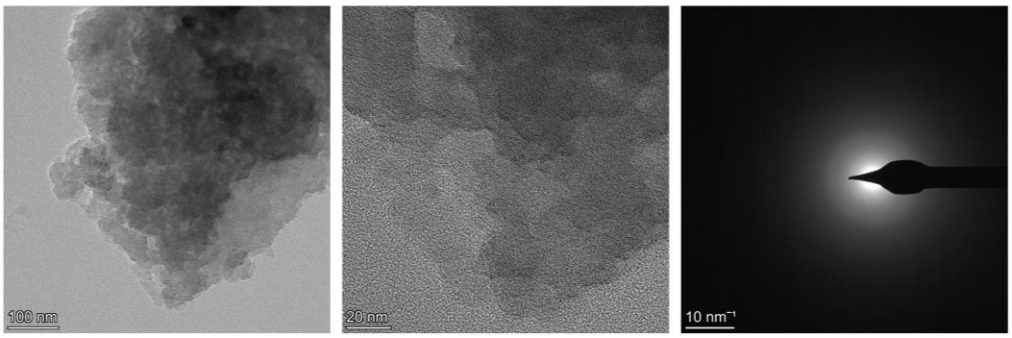

Fig. S28 HR-TEM images of Fe-BTC (left and middle) and associated SAED pattern (right).

10. Basolite F300

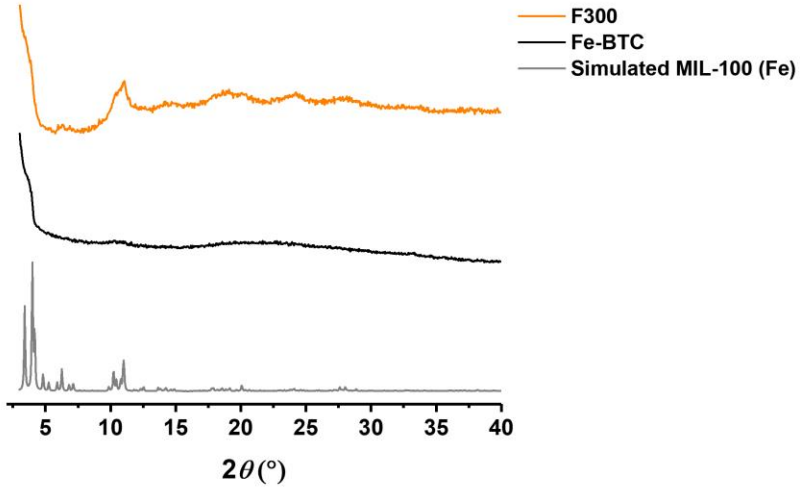

Fig. S29 PXRD patterns of as-synthesized Fe-BTC (black) and F300 (orange) in comparison with a simulated MIL-100 (Fe) pattern (grey).

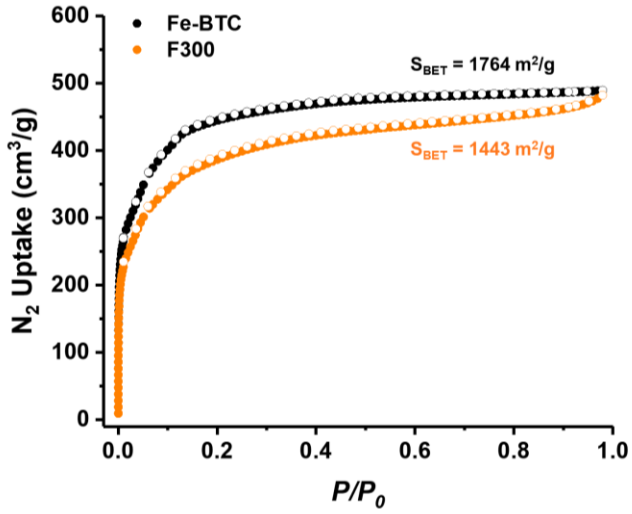

Fig. S30 N_2 adsorption–desorption isotherms (77 K) of Fe-BTC (blank) and F300 (orange).

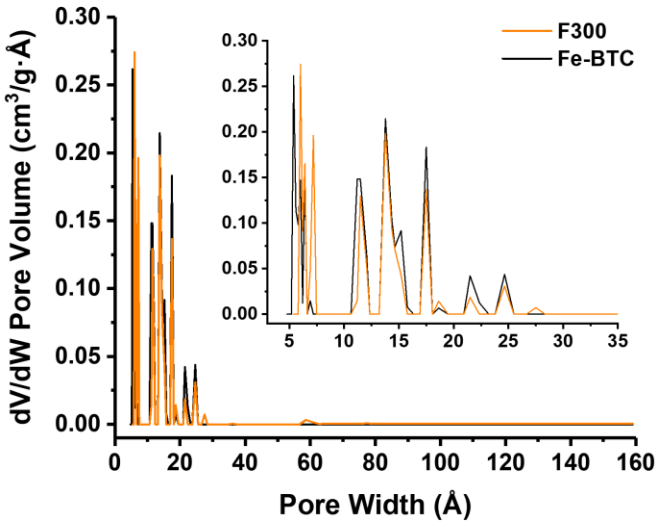

Fig. S31 Pore-size distributions determined from the N_2 adsorption isotherms of Fe-BTC (black) and F300 (orange).

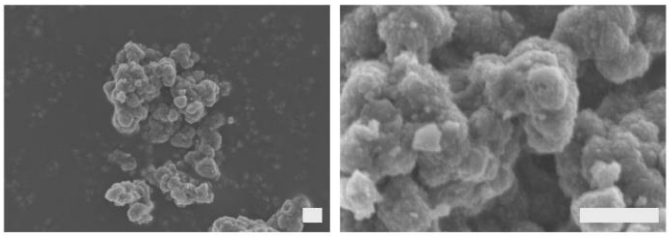

Fig. S32 SEM images of F300. Scale bar, 500 nm.

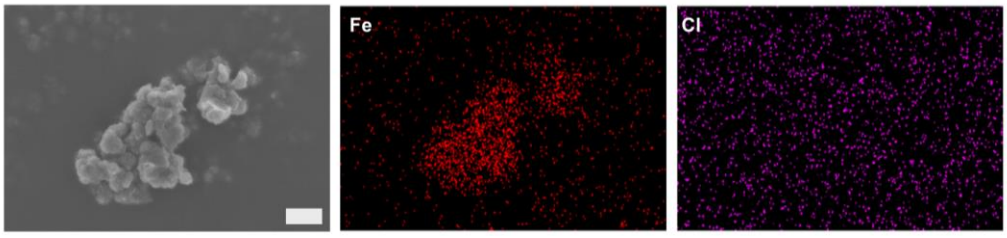

Fig. S33 EDS maps (Fe and Cl) of F300. Scale bar, 500 nm.

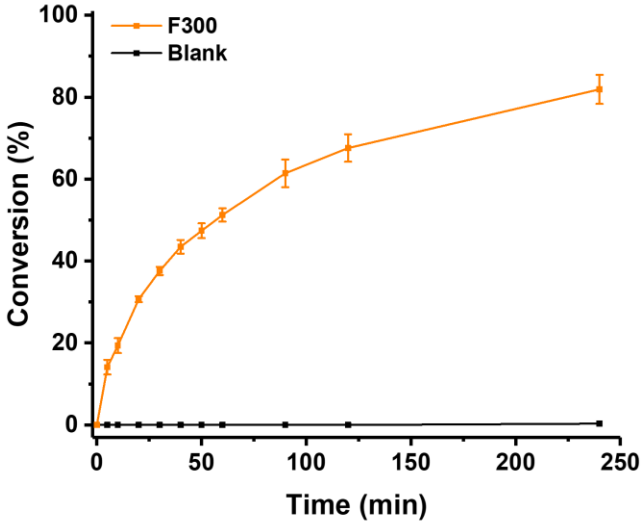

Fig. S34 Deacetalization of benzaldehyde dimethyl acetal catalyzed by F300 (orange) and blank (black).

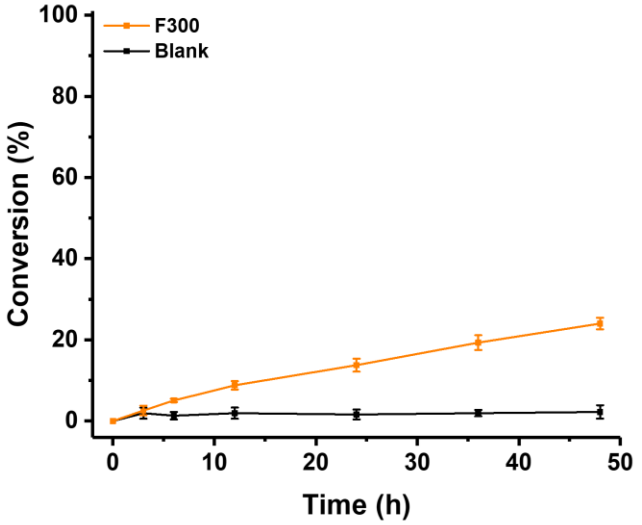

Fig. S35 Knoevenagel condensation of benzaldehyde catalyzed by F300 (orange) and blank (black).

11. Catalyst recycling tests

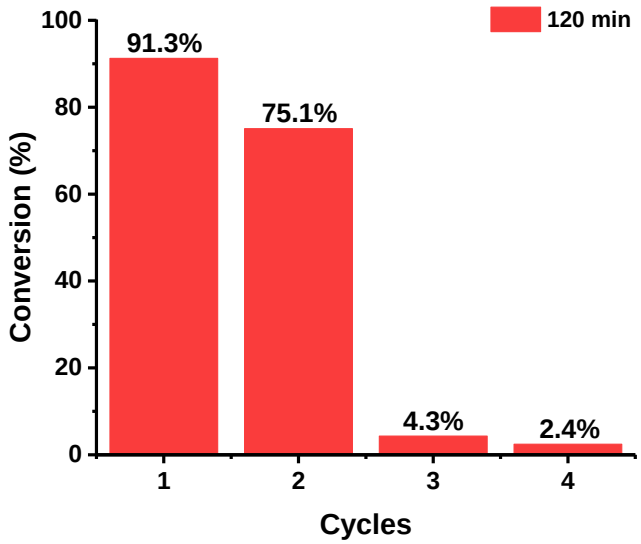

Fig. S36 Fe-BTC recycling test for the deacetalization of benzaldehyde dimethyl acetal at 50 °C for 120 min.

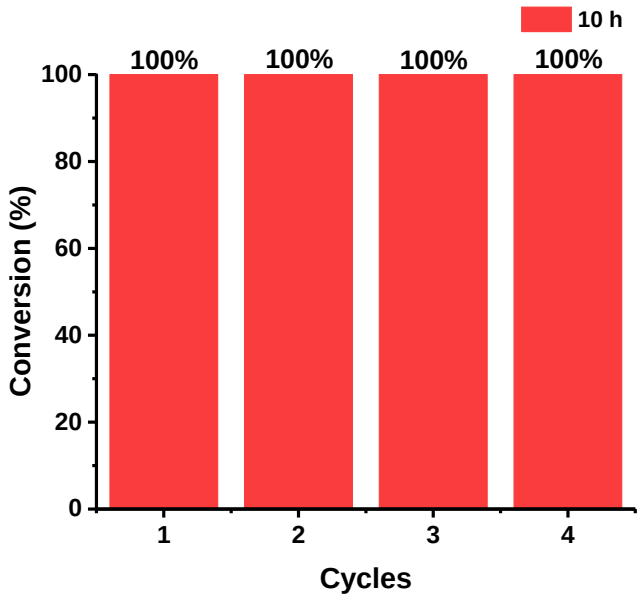

Fig. S37 Fe-BTC recycling test for the cyanosilylation of benzaldehyde at 25 °C for 10 h.

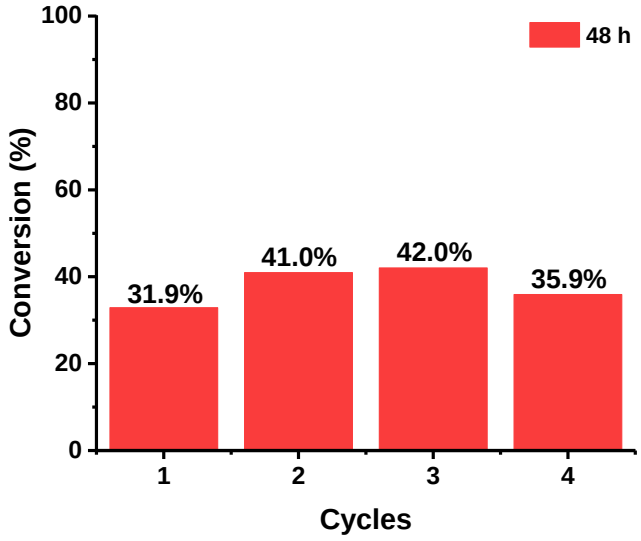

Fig. S38 Fe-BTC recycling test for the Knoevenagel condensation of benzaldehyde at 50 °C for 48 h.

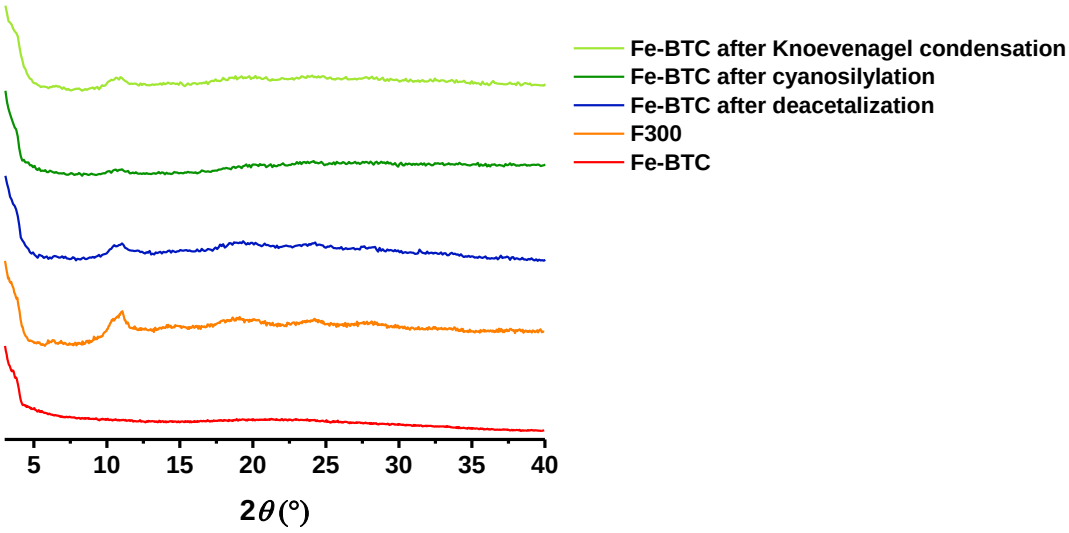

Fig. S39 PXRD patterns of Fe-BTC after the deacetalization (blue), cyanosilylation (green), and Knoevenagel condensation (light green) compared to Fe-BTC (red) and F300 (orange).

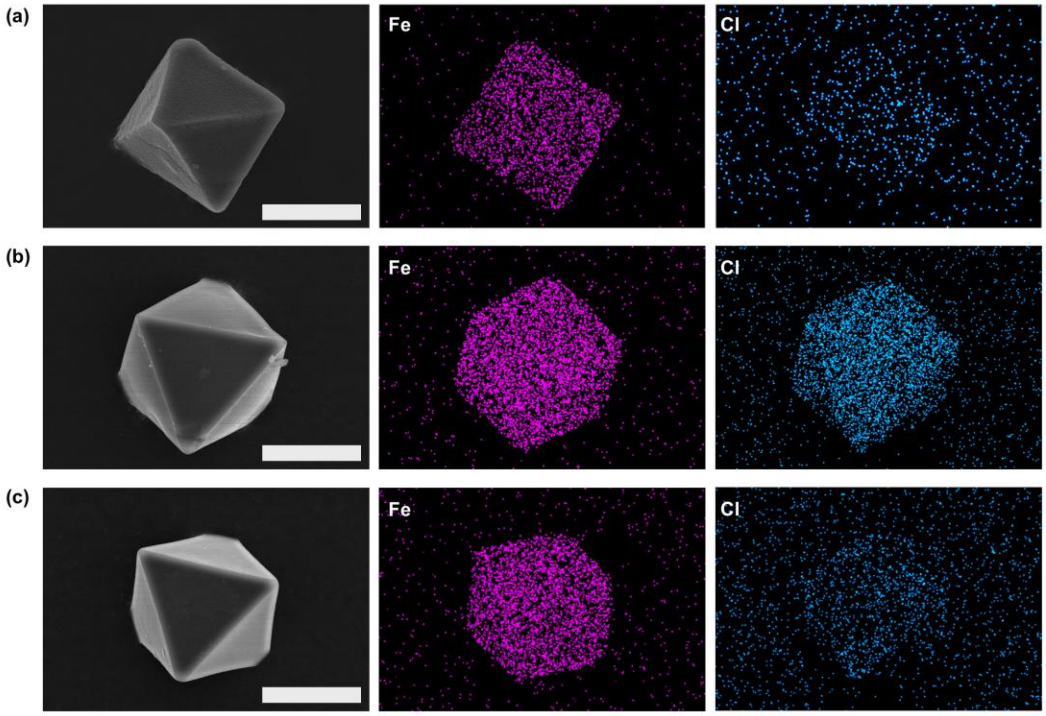

Fig. S40 EDS maps (Fe and Cl) of Fe-BTC after the (a) deacetalization, (b) cyanosilylation, and (c) Knoevenagel condensation reactions. Scale bar, 25 μm.

References

1 B. Lee, Y.-P. Chen, J. Park and J. Park, *ACS Appl. Mater. Interfaces*, 2019, **11**, 25817-25823.

2 X. Song, S. Jeong, D. Kim and M. S. Lah, *CrystEngComm*, 2012, **14**, 5753-5756.

3 J. W. Shin, K. Eom and D. Moon, *J. Synchrotron Radiat.*, 2016, **23**, 369-373.

4 Z. Otwinowski and W. Minor, in *Methods Enzymol.*, Academic Press, 1997, vol. 276, pp. 307-326.

5 G. Sheldrick, *Acta Cryst. C*, 2015, **71**, 3-8.

6 R. S. Muralidhara, C. R. Kesavulu, J. L. Rao, R. V. Anavekar and R. P. S. Chakradhar, *J. Phys. Chem. Solids*, 2010, **71**, 1651-1655.

7 D. Y. Inamdar, A. K. Pathak, I. Dubenko, N. Ali and S. Mahamuni, *J. Phys. Chem. C*, 2011, **115**, 23671-23676.